2024 IEEE/RSJ International Conference on Intelligent Robots and Systems (IROS)
October 14-18, 2024. Abu Dhabi, UAE

Stable Wheel Gait Generation for Planar X-shaped Walker with Telescopic Legs Based on Asymmetric Impact Posture

Fumihiko Asano[1], Mikito Komori[1], Taiki Sedoguchi[1] and Yanqiu Zheng[2]

***Abstract*— This paper introduces a novel X-shaped walker with telescopic legs and investigates its control method with the aim of generating a stable wheel gait on a horizontal plane without including zero dynamics which is essentially unstable and difficult to stabilize. First, we outline a planar 6-DOF robot model with three control inputs, and describe the equations of motion and inelastic collision. Second, we design an output-following control system that smoothly controls the extension/contraction lengths of the legs and relative hip-joint angle to their target terminal values, and creates an asymmetric impact posture in the anteroposterior direction so that the robot can easily overcome the next potential barrier. The coefficients of the desired-time trajectory for each control output are updated with the position and velocity values immediately after each impact as the target initial values, so the generated leg motion and control inputs exhibit smooth time variation. The validity of the proposed gait generation method and the change trend of fundamental motion characteristics with respect to control parameters are investigated through numerical simulations.**

I. INTRODUCTION

The authors are studying the method of a novel bipedal locomotion called wheel gait [1], which is achieved by rotating the stance and swing legs in the same direction. The legged robot introduced as a control object was a model with near-linear characteristics, with the center of mass (COM) of the stance leg, swing leg, and reaction wheel sandwiched between them all being on the central axis [2], [3]. This model also has special properties in that the angular velocity of the rear leg does not change during the collision phase for stance-leg exchange, and that the time integral of the control input for one step becomes zero in the steady gait [4]. In our previous study [5], we also achieved stable wheel gait generation on a horizontal plane using a 3-DOF model of a planar X-shaped walker in which two identical leg frames and a reaction wheel sandwiched between them were connected via a drive shaft passing through each center position. Although the generated motion has the advantage that there is no need to consider the clearance of the swing leg, it is fundamentally difficult to achieve because of the following mechanical contradiction. To generate motion, a relative hip-joint torque is applied between the stance and swing legs, and as a result, both legs are driven in opposite directions. In a wheel gait, however, both legs must rotate in the same direction. Although it was possible to generate a wheel gait by adding a reaction wheel between the legs and using the driving torques, the motion of the reaction wheel behaving as zero dynamics always becomes an unstable periodic orbit and identifying the initial state was not easy.

In order to solve this problem, in this paper, we propose a novel model of a planar X-shaped walker with telescopic legs and without a reaction wheel, and numerically show that stable wheel gait generation is easily achieved by controlling the extension and contraction of the legs and the relative hip-joint angle. Specifically, by controlling the rear leg length to become relatively long and the fore leg length to become relatively short in the impact posture, the entire COM will be closer to the landing point of the fore foot, and the robot can easily overcome the potential barrier that appears at the next mid-stance [6]–[9]. Since the impact posture is always the same, the only hybrid zero dynamics (HZD) for which convergence must be discussed is the angular velocity of the stance leg [10]. First, we outline the model assumptions and develop the mathematical equations of motion and collision. Second, we design an output-following control system and desired-time trajectories. Third, we conduct numerical simulations to clarify the typical wheel gait and fundamental gait properties with respect to the system parameters.

Fig. 1 left shows the blueprint of the X-shaped walker under development, and Fig. 1 right shows a conceptual diagram of a multifunctional robot that combines two X-shaped walkers using a tensegrity structure. Our final goal is to create a multifunctional locomotion robot that can

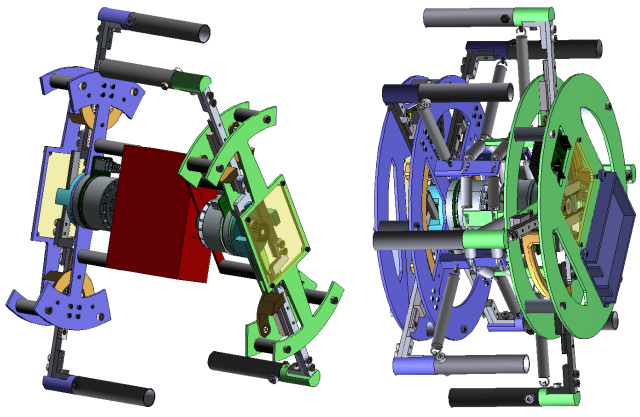

Fig. 1. Experimental X-shaped walker under development (left) and combination of two walkers (right)

This research was partially supported by Grant-in-Aid for Scientific Research (C) No. 23K03727, provided by the Japan Society for the Promotion of Science (JSPS).

[1]F. Asano, M. Komori and T. Sedoguchi are with the Graduate School of Advanced Science and Technology, Japan Advanced Institute of Science and Technology, 1-1 Asahidai, Nomi, Ishikawa 923-1292, Japan {fasano,s2310055,sedoguchi}@jaist.ac.jp

[2]Y. Zheng is with the Department of Mechanical Engineering, Ritsumeikan University, 1-1-1 Nojihigashi, Kusatsu, Shiga 525-8577, Japan zhengyq@fc.ritsumei.ac.jp

combine or separate the X-shaped walker as the minimal component depending on the environment and work purpose. This is an advanced legged locomotion system that can be combined in situations where multi-legged locomotion mode is advantageous, and separated when it is necessary to increase the number of robots and perform cooperative work. It is expected to be useful in a variety of situations. This paper provides a thorough discussion of the mathematical model and motion characteristics when the X-shaped walker moves independently.

II. MODELING

A. Equation of Motion

In the following, the subscript $j \in \{1, 2\}$ shall represent the number of the leg frame; 1 for the stance leg, and 2 for the swing leg. Fig. 2 left shows an overview of the planar telescopic-legged X-shaped walker treated in this paper, and Fig. 2 right explains the detailed coordinate system of the leg frame j. Here, (x, z) is the lower end position of the stance leg; θ_j is the absolute angle of the leg frame j; b_j is the extension/contraction length of the leg frame j; the distance from the leg end to the mass $m_1/2$ is a; the distance from the mass $m_2/2$ to the rotational joint is c. Define the length from the rotational joint to the leg end as $L_j := a + b_j + c$. The total mass of one leg frame is $m_1 + m_2$, and the total length of it is $2L_j$. Furthermore, around the rotational joint, it is possible to apply a control torque u_3 from the swing leg to the stance leg.

We assume that the robot has the following body structure and mechanism. Two straight base links with a mass of m_2 are connected via the rotary axis (hip joint) located at the same position as their COM, and two straight foot links with a mass of $m_1/2$ are attached on both sides of the base link so that they can extend and contract symmetrically along it. By using the internal transmission mechanism, it is possible to simultaneously apply a driving force to the telescopic joints on both sides, so that the two foot links move symmetrically in opposite directions. As a result of this symmetrical movement, the COM of each leg frame as a whole is always located at the same central position as the hip joint.

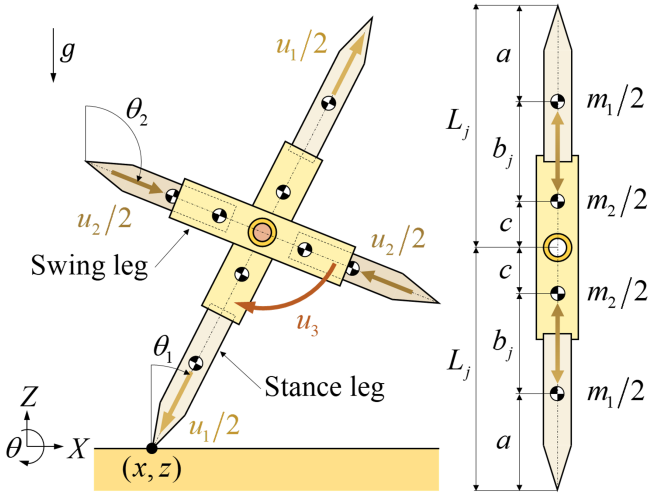

Fig. 2. Model of planar X-shaped walker with telescopic legs

Let $\boldsymbol{q} = \begin{bmatrix} x & z & \theta_1 & \theta_2 & b_1 & b_2 \end{bmatrix}^{\mathrm{T}}$ be the generalized coordinate vector. The robot equation of motion then becomes

$$\boldsymbol{M}\ddot{\boldsymbol{q}} + \boldsymbol{h} = \boldsymbol{S}\boldsymbol{u} + \boldsymbol{J}_c^{\mathrm{T}}\boldsymbol{\lambda}_c, \tag{1}$$

where $\boldsymbol{M} \in \mathbb{R}^6$ is the inertia matrix and $\boldsymbol{h} \in \mathbb{R}^6$ is the nonlinear velocity and gravity term vector. They are detailed as follows.

$$\boldsymbol{M} = \begin{bmatrix} m & 0 & mL_1\cos\theta_1 & 0 & m\sin\theta_1 & 0 \\ & m & -mL_1\sin\theta_1 & 0 & m\cos\theta_1 & 0 \\ & & M_{33} & 0 & 0 & 0 \\ & & & M_{44} & 0 & 0 \\ & & & & m' & 0 \\ \text{Sym.} & & & & & m_1 \end{bmatrix} \tag{2}$$

$$\begin{aligned} m &= 2m_1 + 2m_2, \quad m' = 3m_1 + 2m_2 \\ M_{33} &= 3m_1(b_1 + c)^2 + m_2\left(2b_1^2 + 4b_1c + 3c^2\right) + ma^2 \\ &\quad +2ma(b_1 + c) \\ M_{44} &= m_1\left(b_2 + c\right)^2 + m_2c^2 \end{aligned}$$

$$\boldsymbol{h} = \begin{bmatrix} m\dot{\theta}_1\left(2\dot{b}_1\cos\theta_1 - L_1\dot{\theta}_1\sin\theta_1\right) \\ m\left(g - L_1\dot{\theta}_1^2\cos\theta_1 - 2\dot{b}_1\dot{\theta}_1\sin\theta_1\right) \\ -mgL_1\sin\theta_1 + 2\dot{b}_1\dot{\theta}_1\left(ma + m'(b_1 + c)\right) \\ 2m_1\dot{b}_2\dot{\theta}_2(b_2 + c) \\ mg\cos\theta_1 - \left(ma + m'(b_1 + c)\right)\dot{\theta}_1^2 \\ -m_1(b_2 + c)\dot{\theta}_2^2 \end{bmatrix} \tag{3}$$

The first term on the right side of Eq. (1) is the control input vector, and is detailed as follows.

$$\boldsymbol{S} = \begin{bmatrix} 0 & 0 & 0 \\ 0 & 0 & 0 \\ 0 & 0 & 1 \\ 0 & 0 & -1 \\ 1 & 0 & 0 \\ 0 & 1 & 0 \end{bmatrix}, \quad \boldsymbol{u} = \begin{bmatrix} u_1 \\ u_2 \\ u_3 \end{bmatrix} \tag{4}$$

Note that, however, u_1 and u_2 here refer to the total driving forces of the two telescopic joints of the stance leg and the swing leg, respectively. In Fig. 2, it is simply shown as $u_j/2$ to match the halved mass $m_1/2$, but in reality it is not equally distributed.

The second term on the right side of Eq. (1) is the holonomic constraint force term, and the undetermined multiplier vector $\boldsymbol{\lambda}_c \in \mathbb{R}^2$ represents the ground reaction force vector. We assume that the stance foot is always in contact with the ground without sliding, and the velocity constraint conditions are specified as $\dot{x} = 0$ and $\dot{z} = 0$. By summarizing these, we obtain

$$\boldsymbol{J}_c\dot{\boldsymbol{q}} = \boldsymbol{0}_{2\times 1}, \quad \boldsymbol{J}_c = \begin{bmatrix} 1 & 0 & 0 & 0 & 0 & 0 \\ 0 & 1 & 0 & 0 & 0 & 0 \end{bmatrix}. \tag{5}$$

Following Eq. (1) and the time derivative of Eq. (5), we obtain

$$\boldsymbol{\lambda}_c = -\boldsymbol{X}_c^{-1}\boldsymbol{J}_c\boldsymbol{M}^{-1}\left(\boldsymbol{S}\boldsymbol{u} - \boldsymbol{h}\right) = \begin{bmatrix} F_x \\ F_z \end{bmatrix}, \tag{6}$$

where $\boldsymbol{X}_c := \boldsymbol{J}_c\boldsymbol{M}^{-1}\boldsymbol{J}_c^{\mathrm{T}}$, and F_x and F_z are the X-

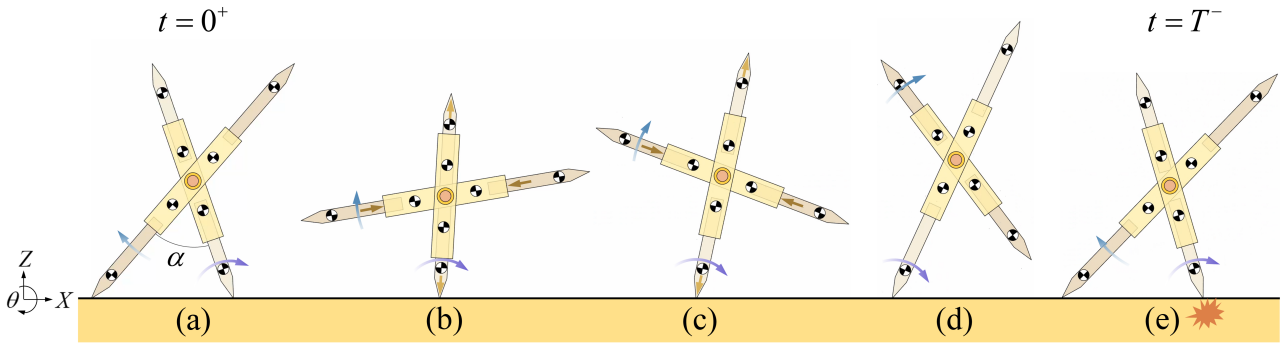

Fig. 3. Motion sequence in wheel gait for one step

and Z-direction components of the ground reaction force. A necessary condition for generating a stable wheel gait is that F_z is always maintained at a positive value during motion. By substituting Eq. (6) into Eq. (1) and arranging it, we finally obtain

$$\boldsymbol{M}\ddot{\boldsymbol{q}} = \boldsymbol{Y}_c\left(\boldsymbol{S}\boldsymbol{u} - \boldsymbol{h}\right), \tag{7}$$

where $\boldsymbol{Y}_c := \boldsymbol{I}_6 - \boldsymbol{J}_c^{\mathrm{T}}\boldsymbol{X}_c^{-1}\boldsymbol{J}_c\boldsymbol{M}^{-1}$.

B. Collision Equation for Stance-leg Exchange

In this paper, we discuss a method for generating the wheel gait motion shown in Fig. 3. Let t be the time parameter reset to zero at every instant of stance-leg exchange, and T be the step period defined as the time interval from the stance-leg exchange to the next. The robot starts its movement from an asymmetric impact posture tilted forward at $t = 0$ as shown in Fig. 3(a), creates the next impact posture during the single support phase while rotating both the two leg frames clockwise, and falls down as a 1-DOF rigid body. We assume that, in each collision phase, the telescopic lengths of the rear and fore legs are controlled to b_s and b_e ($b_s < b_e$), and the relative hip-joint angle is controlled to α with sufficient accuracy. We also assume that, when the swing leg lands at $t = T$ as shown in Fig. 3(e), the end position makes a completely inelastic collision with the ground without slipping or bouncing, and that the rear foot leaves the ground immediately after that.

By setting the coordinate system at the instant of fore-foot landing as shown in Fig. 4, the collision equation becomes

$$\boldsymbol{M}\dot{\boldsymbol{q}}^+ = \boldsymbol{M}\dot{\boldsymbol{q}}^- + \boldsymbol{J}_I^{\mathrm{T}}\boldsymbol{\lambda}_I. \tag{8}$$

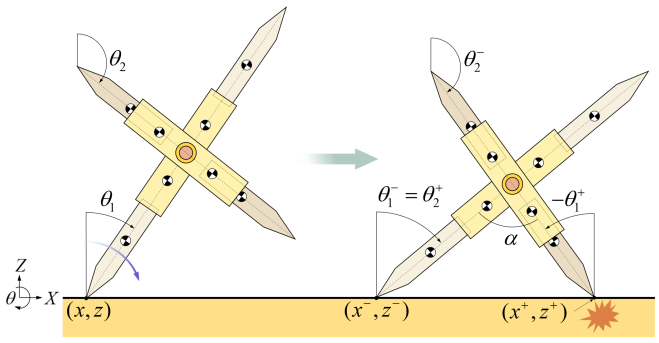

Fig. 4. Configuration at instant of stance-leg exchange

Here, the superscripts "$-$" and "$+$" shall denote immediately before and immediately after impact, and $\boldsymbol{\lambda}_I \in \mathbb{R}^2$ represents the impulse vector determined as the zero-time integral of impulse force. The velocity constraint condition that should hold regarding the fore foot position immediately after landing becomes

$$\boldsymbol{J}_I\dot{\boldsymbol{q}}^+ = \boldsymbol{0}_{2\times 1}, \tag{9}$$

where the detail of the Jacobian matrix $\boldsymbol{J}_I$ is

$$\boldsymbol{J}_I = \begin{bmatrix} 1 & 0 & L_1^- \cos\theta_1^- & L_2^- \cos\theta_2^- & \sin\theta_1^- & \sin\theta_2^- \\ 0 & 1 & -L_1^- \sin\theta_1^- & -L_2^- \sin\theta_2^- & \cos\theta_1^- & \cos\theta_2^- \end{bmatrix}. \tag{10}$$

Following Eqs. (8) and (9), we obtain the velocity vector immediately after impact as

$$\dot{\boldsymbol{q}}^+ = \left(\boldsymbol{I}_6 - \boldsymbol{M}^{-1}\boldsymbol{J}_I^{\mathrm{T}}\left(\boldsymbol{J}_I\boldsymbol{M}^{-1}\boldsymbol{J}_I^{\mathrm{T}}\right)^{-1}\boldsymbol{J}_I\right)\dot{\boldsymbol{q}}^-. \tag{11}$$

After completing the above calculations, update each component in the $\boldsymbol{q}^+$ and $\dot{\boldsymbol{q}}^+$ vectors as follows, taking into account the stance-leg exchange.

$$\begin{bmatrix} x^+ \\ z^+ \\ \theta_1^+ \\ \theta_2^+ \\ b_1^+ \\ b_2^+ \end{bmatrix} = \begin{bmatrix} 0 \\ 0 \\ \theta_2^- - \pi \\ \theta_1^- \\ b_2^- \\ b_1^- \end{bmatrix}, \quad \begin{bmatrix} \dot{x}^+ \\ \dot{z}^+ \\ \dot{\theta}_1^+ \\ \dot{\theta}_2^+ \\ \dot{b}_1^+ \\ \dot{b}_2^+ \end{bmatrix} = \begin{bmatrix} 0 & 0 & 0 & 0 & 0 & 0 \\ 0 & 0 & 0 & 0 & 0 & 0 \\ 0 & 0 & 0 & 1 & 0 & 0 \\ 0 & 0 & 1 & 0 & 0 & 0 \\ 0 & 0 & 0 & 0 & 0 & 1 \\ 0 & 0 & 0 & 0 & 1 & 0 \end{bmatrix} \dot{\boldsymbol{q}}^+ \tag{12}$$

In Eq. (11), the relationship $\dot{\theta}_1^+ = \dot{\theta}_1^-$ holds; that is, even if the robot has telescopic legs or the impact posture is not symmetrical, the angular velocity of the rear leg does not change during the collision phase [1]–[4]. By combining this characteristic with the features of the output-following control system described in the next section, it is expected that a very smooth wheel gait will be generated.

III. CONTROL SYSTEM DESIGN

A. Input-output Linearization

Let $\theta_H := \theta_1 - \theta_2$ be the relative hip-joint angle, and define the control-output vector as

$$\boldsymbol{y} := \boldsymbol{S}^{\mathrm{T}}\boldsymbol{q} = \begin{bmatrix} b_1 \\ b_2 \\ \theta_H \end{bmatrix}. \tag{13}$$

The second-order derivative with respect to time then becomes

$$\ddot{\boldsymbol{y}} = \boldsymbol{S}^{\mathrm{T}}\ddot{\boldsymbol{q}} = \boldsymbol{S}^{\mathrm{T}}\boldsymbol{M}^{-1}\boldsymbol{Y}_c\left(\boldsymbol{S}\boldsymbol{u} - \boldsymbol{h}\right). \tag{14}$$

Define the desired control output vector as

$$\boldsymbol{y}_{\mathrm{d}}(t) = \begin{bmatrix} b_{1\mathrm{d}}(t) \\ b_{2\mathrm{d}}(t) \\ \theta_{H\mathrm{d}}(t) \end{bmatrix}. \tag{15}$$

Then, we can determine the control input for achieving $\boldsymbol{y} \to \boldsymbol{y}_{\mathrm{d}}(t)$ as

$$\boldsymbol{u} = \left(\boldsymbol{S}^{\mathrm{T}}\boldsymbol{M}^{-1}\boldsymbol{Y}_c\boldsymbol{S}\right)^{-1}\left(\boldsymbol{v} + \boldsymbol{S}^{\mathrm{T}}\boldsymbol{M}^{-1}\boldsymbol{Y}_c\boldsymbol{h}\right), \tag{16}$$

$$\boldsymbol{v} = \ddot{\boldsymbol{y}}_{\mathrm{d}}(t) + \boldsymbol{K}_D\left(\dot{\boldsymbol{y}}_{\mathrm{d}}(t) - \dot{\boldsymbol{y}}\right) + \boldsymbol{K}_P\left(\boldsymbol{y}_{\mathrm{d}}(t) - \boldsymbol{y}\right), \tag{17}$$

where $\boldsymbol{K}_D = k_d\boldsymbol{I}_3$ is the derivative gain matrix, $\boldsymbol{K}_P = k_p\boldsymbol{I}_3$ is the proportional gain matrix, k_d and k_p are positive constants, and $\boldsymbol{v}$ is the desired acceleration command signal vector.

B. Design of Desired-time Trajectories

Let T_{set} be the target settling time. In the wheel gait generation, we consider the following control strategy. At $t = 0$ or immediately after stance-leg exchange, b_1 is b_s, b_2 is b_e, and θ_H is α. Then, we smoothly expand b_1 to reach b_e and contract b_2 to reach b_s at $t = T_{\mathrm{set}}$. We also smoothly control θ_H to reach $\alpha - \pi$ at $t = T_{\mathrm{set}}$. When achieving limit cycle walking by performing control to follow desired-time trajectories, a problem always arises; a very large control input is generated due to the tracking error between the actual speed and its target value immediately after stance-leg exchange. To solve this problem, we set the target initial position and velocity values to their actual values immediately after stance-leg exchange. The target acceleration values are, however, set to zero.

$$\begin{aligned} b_{1\mathrm{d}}(0) &= b_1^+, \quad \dot{b}_{1\mathrm{d}}(0) = \dot{b}_1^+, \quad \ddot{b}_{1\mathrm{d}}(0) = 0 \\ b_{2\mathrm{d}}(0) &= b_2^+, \quad \dot{b}_{2\mathrm{d}}(0) = \dot{b}_2^+, \quad \ddot{b}_{2\mathrm{d}}(0) = 0 \\ \theta_{H\mathrm{d}}(0) &= \theta_H^+, \quad \dot{\theta}_{H\mathrm{d}}(0) = \dot{\theta}_H^+, \quad \ddot{\theta}_{H\mathrm{d}}(0) = 0 \end{aligned}$$

We also set their target terminal values to the followings.

$$\begin{aligned} b_{1\mathrm{d}}(T_{\mathrm{set}}) &= b_e, \quad \dot{b}_{1\mathrm{d}}(T_{\mathrm{set}}) = 0, \quad \ddot{b}_{1\mathrm{d}}(T_{\mathrm{set}}) = 0 \\ b_{2\mathrm{d}}(T_{\mathrm{set}}) &= b_s, \quad \dot{b}_{2\mathrm{d}}(T_{\mathrm{set}}) = 0, \quad \ddot{b}_{2\mathrm{d}}(T_{\mathrm{set}}) = 0 \\ \theta_{H\mathrm{d}}(T_{\mathrm{set}}) &= \alpha - \pi, \quad \dot{\theta}_{H\mathrm{d}}(T_{\mathrm{set}}) = 0, \quad \ddot{\theta}_{H\mathrm{d}}(T_{\mathrm{set}}) = 0 \end{aligned}$$

After T_{set}, each control output is fixed to maintain its target terminal value, and the robot falls down as a 1-DOF rigid body. As desired-time trajectories that satisfy the above conditions, we introduce the following fifth-order functions for the control outputs.

$$b_{1\mathrm{d}}(t) = \begin{cases} \sum_{k=0}^{5}\xi_k t^k & (0 \le t < T_{\mathrm{set}}) \\ b_e & (t \ge T_{\mathrm{set}}) \end{cases} \tag{18}$$

$$b_{2\mathrm{d}}(t) = \begin{cases} \sum_{k=0}^{5}\eta_k t^k & (0 \le t < T_{\mathrm{set}}) \\ b_s & (t \ge T_{\mathrm{set}}) \end{cases} \tag{19}$$

$$\theta_{H\mathrm{d}}(t) = \begin{cases} \sum_{k=0}^{5}\zeta_k t^k & (0 \le t < T_{\mathrm{set}}) \\ \alpha - \pi & (t \ge T_{\mathrm{set}}) \end{cases} \tag{20}$$

The coefficients in the above equations can be determined as

$$\begin{bmatrix} \xi_2 & \eta_2 & \zeta_2 \\ \xi_1 & \eta_1 & \zeta_1 \\ \xi_0 & \eta_0 & \zeta_0 \end{bmatrix} = \begin{bmatrix} 0 & 0 & 0 \\ \dot{b}_1^+ & \dot{b}_2^+ & \dot{\theta}_H^+ \\ b_1^+ & b_2^+ & \theta_H^+ \end{bmatrix}, \quad \begin{bmatrix} \xi_5 & \eta_5 & \zeta_5 \\ \xi_4 & \eta_4 & \zeta_4 \\ \xi_3 & \eta_3 & \zeta_3 \end{bmatrix} = \boldsymbol{\Phi}^{-1}\boldsymbol{\Gamma}, \tag{21}$$

where

$$\boldsymbol{\Phi} = \begin{bmatrix} T_{\mathrm{set}}^5 & T_{\mathrm{set}}^4 & T_{\mathrm{set}}^3 \\ 5T_{\mathrm{set}}^4 & 4T_{\mathrm{set}}^3 & 3T_{\mathrm{set}}^2 \\ 20T_{\mathrm{set}}^3 & 12T_{\mathrm{set}}^2 & 6T_{\mathrm{set}} \end{bmatrix}, \tag{22}$$

$$\boldsymbol{\Gamma} = \begin{bmatrix} b_e - \dot{b}_1^+ T_{\mathrm{set}} - b_1^+ & -\dot{b}_1^+ & 0 \\ b_s - \dot{b}_2^+ T_{\mathrm{set}} - b_2^+ & -\dot{b}_2^+ & 0 \\ \alpha - \pi - \dot{\theta}_H^+ T_{\mathrm{set}} - \theta_H^+ & -\dot{\theta}_H^+ & 0 \end{bmatrix}^{\mathrm{T}}. \tag{23}$$

In this paper, one of the necessary conditions for stable wheel gait generation is that T_{set} is always shorter than T, that is, the output settling control to the target terminal values is completed by the instant of the next fore-foot landing.

IV. WHEEL GAIT ANALYSIS

A. Preliminaries to Analysis

The energy efficiency of the generated wheel gait can be evaluated in terms of specific resistance (SR). Define the average input power, p, as

$$p := \frac{1}{T}\int_{0^+}^{T^-}\left(\left|\dot{b}_1 u_1\right| + \left|\dot{b}_2 u_2\right| + \left|\dot{\theta}_H u_3\right|\right)\mathrm{d}t. \tag{24}$$

Then SR is defined as $\mathrm{SR} := p/mgv$, where v is the walking speed and is calculated as the step length divided by the step period. SR is a dimensionless quantity that represents the energy consumed to move 1 kilogram of mass by 1 meter, and the smaller this value, the better the gait efficiency. The step length, Δx, is defined as the distance between the rear and fore feet at impact. Assuming that all control outputs are settled to their respective target terminal values with sufficient accuracy, using the cosine formula, the value can be calculated analytically as

$$\begin{aligned} (\Delta x)^2 = {} & (a + b_e + c)^2 + (a + b_s + c)^2 \\ & -2\left(a + b_e + c\right)\left(a + b_s + c\right)\cos\alpha. \end{aligned} \tag{25}$$

The partial derivative of Δx with respect to α becomes

$$\frac{\partial \Delta x}{\partial \alpha} = \frac{\left(a + b_e + c\right)\left(a + b_s + c\right)\sin\alpha}{\Delta x} > 0, \tag{26}$$

and we can understand that Δx increases monotonically as α increases.

B. Typical Wheel Gait

Fig. 5 shows the simulation results of wheel gait generation of the planar X-shaped walker. Here, (a) is the angular positions of the legs, (b) the telescopic lengths, (c) the control input forces, u_1 and u_2, (d) the control input torque, u_3, and (e) the ground reaction forces. The physical and control parameters were chosen as the values listed in Table I. The

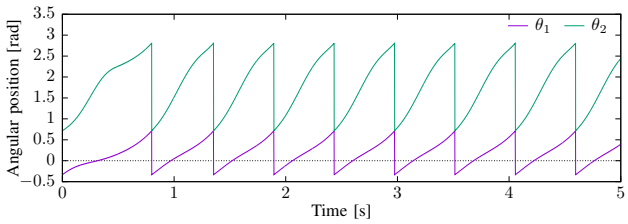

(a) Angular position

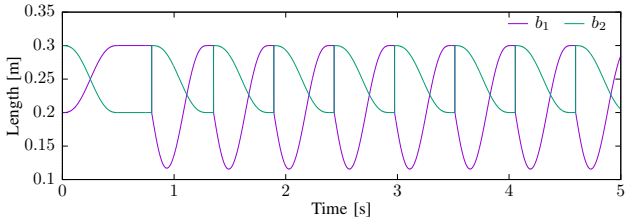

(b) Telescopic length

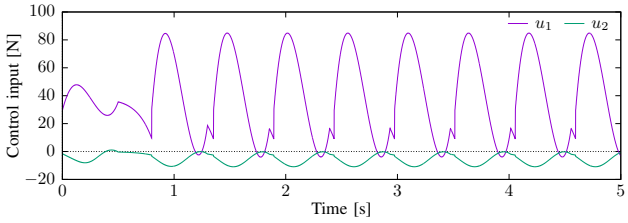

(c) Control input (expansion and contraction force)

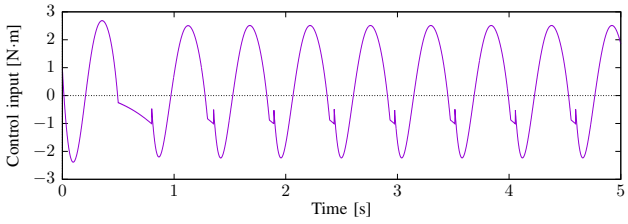

(d) Control input (hip-joint torque)

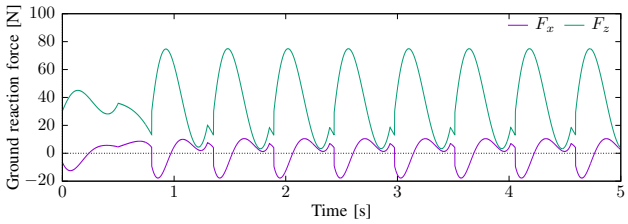

(e) Ground reaction force

Fig. 5. Simulation results of stable wheel gait generation of telescopic-legged X-shaped walker

initial state was also set as

$$\boldsymbol{q}(0) = \begin{bmatrix} 0 \\ 0 \\ \tan^{-1}\left(\frac{L_2\cos\alpha - L_1}{L_2\sin\alpha}\right) \\ \tan^{-1}\left(\frac{L_2\cos\alpha - L_1}{L_2\sin\alpha}\right) + \alpha \\ b_s \\ b_e \end{bmatrix}, \quad \dot{\boldsymbol{q}}(0) = \begin{bmatrix} 0 \\ 0 \\ \dot{\theta}_1(0) \\ \dot{\theta}_1(0) \\ 0 \\ 0 \end{bmatrix}, \tag{27}$$

where $\dot{\theta}_1(0)$ is the initial angular velocity, and must have a value large enough to overcome the first potential barrier. We set it to 2.0 [rad/s] here. From the simulation results, we can see that a stable wheel gait could be generated on the horizontal plane. From Figs. 5(c) and (d), we can see that by updating the initial values of the positions and velocities in the target trajectories immediately after each stance-leg exchange, smooth control inputs were generated without causing any trajectory tracking errors. As a result, the ground reaction forces change smoothly, as shown in Fig. 5(e). The most characteristic movement is that, as shown in Fig. 5(b), the telescopic length of the stance (fore) leg begins to contract rapidly immediately after the stance-leg exchange. This high leg compliance makes the entire walking motion smooth and effortless. Although not discussed in this paper, it is expected that by attaching elastic elements to each telescopic joint, energy efficiency would be improved and it would also be possible to achieve running motion.

TABLE I

PHYSICAL AND CONTROL PARAMETERS

m_1	1.0	kg	$T_{\rm set}$	0.5	s
m_2	1.0	kg	b_s	0.2	m
a	0.1	m	b_e	0.3	m
c	0.1	m	k_d	100	$\rm s^{-1}$
α	$\frac{\pi}{3}$	rad	k_p	2500	$\rm s^{-2}$

C. *Effect of* α *and* $T_{\rm set}$

Fig. 6 shows the analysis results of the gait descriptors in the generated wheel gaits for seven values of $T_{\rm set}$ with respect to α. Here, (a) is the step period, (b) the walking speed, and (c) the specific resistance. The system parameters other than $T_{\rm set}$ and α were chosen as the values listed in Table I again. All generated wheel gaits were asymptotically stable and period-1, but we judged it to be successful only if the following three conditions were met.

- The step period was longer than the desired settling time, that is, $T \geq T_{\rm set}$ was satisfied.
- The vertical ground reaction force of the stance leg, F_z, was always maintained to be positive.
- Once the rear foot took off immediately after the stance-leg exchange, it did not touch the ground again.

From the results, we can see that the step period in all cases monotonically increases with respect to α. As previously mentioned, the step period also monotonically increases with respect to α regardless of $T_{\rm set}$, but since the influence of the step period is greater, the walking speed results in a monotonous decrease. By applying the output-following control system described in the previous section, all control outputs were precisely settled to their respective target terminal values without causing trajectory tracking errors, and the step lengths matched the calculated value by theoretical formula (25). Therefore, we omitted the display of the results here. As α increases, the step length increases, but this also results in the impact posture not leaning forward, so it becomes more difficult to overcome the potential barrier and the walking speed decreases.

The SR shown in Fig. 6 shows the most complex change trend. When $T_{\rm set}$ is small, it shows a monotonous decreasing

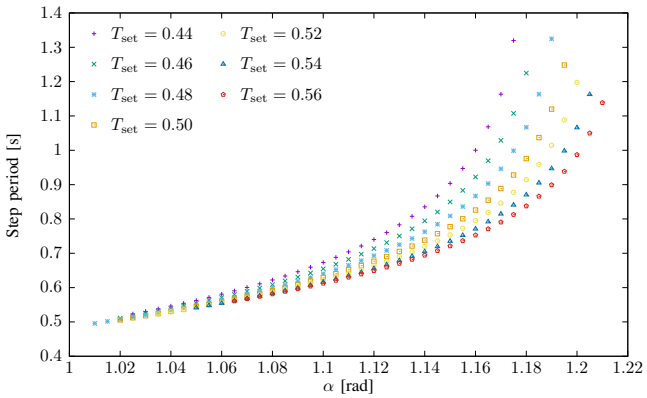

(a) Step period

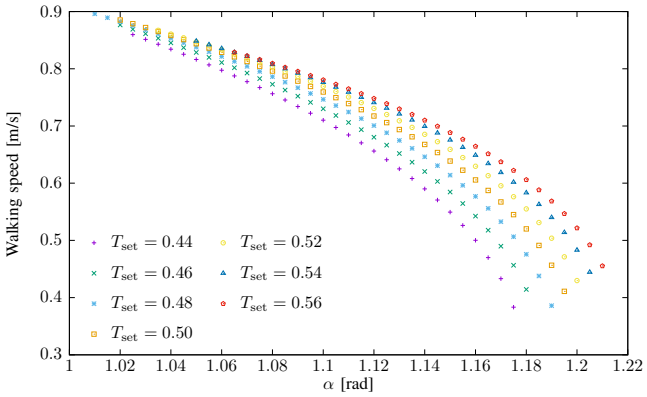

(b) Walking speed

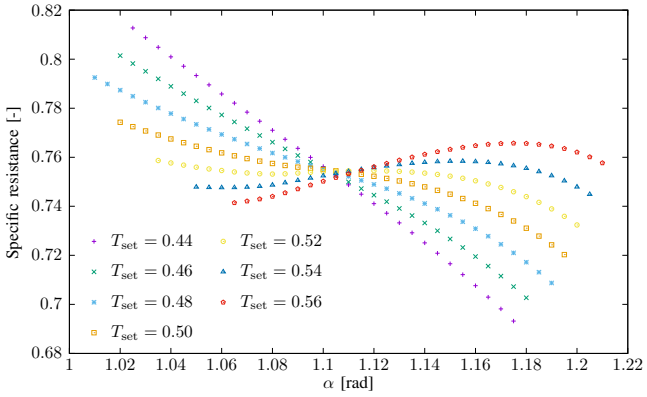

(c) Specific resistance

Fig. 6. Gait descriptors in generated wheel gaits for seven values of $T_{\rm set}$ with respect to α

tendency as α increases, but when $T_{\rm set}$ is large, it increases once and then starts decreasing. For all $T_{\rm set}$ cases, there is a tendency for SR to pass through a value of approximately 0.76 when α is approximately 1.1. On the other hand, the SR value is relatively large for a limit cycle walking robot, and it cannot be said that efficient motion generation has been achieved.

The larger $T_{\rm set}$ is, the larger the lower limit value of the step period is due to the necessity of satisfying the settling-time condition, and therefore the lower limit value of α is also increased accordingly. Conversely, the smaller $T_{\rm set}$ is, the smaller the lower limit of the step period is, but in this case, the cause of the failure to walk was that the generated motion became faster and the vertical ground reaction force became negative during motion.

V. CONCLUSION AND FUTURE WORK

In this paper, we proposed the model of a planar X-shaped walker with telescopic leg frames, designed the output-following control system that makes the leg extension/contraction lengths and relative hip-joint angle follow their desired-time trajectories, and numerically showed that generating a stable wheel gait on a horizontal plane is possible by asymmetrizing the impact posture in the anteroposterior direction. By setting α to a smaller value and making the robot walk with a shorter step length, the walking speed increases, but the energy efficiency does not necessarily improve, and there is also a problem that the settling-time condition cannot be met and the vertical ground reaction force becomes negative during motion.

The robot model treated in this paper has a special property in that its entire COM is always located at the same position as the hip joint, so it may be easier to mathematically consider the relationship between the asymmetric impact posture, restored mechanical energy, and effect of parametric excitation [8], [9]. The physical meaning of the robot equation of motion is equivalent to a 2-DOF system in which a disk with variable inertia is attached to an inverted pendulum with variable inertia. From this perspective, we will further investigate the mathematical meaning of the equations and propose control laws based on the understanding. We would like to complete the experimental machine currently under development as soon as possible and report the results of basic experiments in a future paper.

REFERENCES

[1] J. Kiefer and B. Ramesh, "Walking viability and gait synthesis for a novel class of dynamically-simple bipeds." *Informatica*, Vol. 17, Iss. 2, pp. 145–155, 1993.

[2] M. W. Spong, R. Lozano and R. Mahony, "An almost linear biped," *Proc. of the 39th IEEE Conf. on Decision and Control*, pp. 4803–4808, 2000.

[3] T. G. McGee and M. W. Spong, "Trajectory planning and control of a novel walking biped," *Proc. of the IEEE Int. Conf. on Control Applications*, pp. 1099–1104, 2001.

[4] F. Asano and C. Yan, "Low-speed limit cycle walking of planar X-shaped bipedal robot with special properties," *Proc. of the 8th IEEE Int. Conf. on Advanced Robotics and Mechatronics*, pp. 43–48, 2023.

[5] F. Asano, T. Sedoguchi and C. Yan, "Generation of steady wheel gait for planar X-shaped walker with reaction wheel," *Proc. of the 2024 IEEE International Conference on Robotics and Automation*, pp. 5766–5772, 2024.

[6] F. Asano, "Dynamic gait generation of telescopic-legged rimless wheel based on asymmetric impact posture," *Proc. of the 9th IEEE-RAS Int. Conf. on Humanoid Robots*, pp. 68–73, 2009.

[7] F. Asano, "High-speed biped gait generation based on asymmetrization of impact posture using telescopic legs," *Proc. of the IEEE/RSJ Int. Conf. on Intelligent Robots and Systems*, pp. 4477–4482, 2010.

[8] H. Dong, M. Zhao and N. Zhang, "High-speed and energy-efficient biped locomotion based on virtual slope walking," *Autonomous Robots*, Vol. 30, pp. 199–216, 2011.

[9] Z. Li, K. Deng and M. Zhao, "Powered walking based on the passive dynamic principles: A virtual slope walking approach," *Proc. of the 14th IEEE-RAS Int. Conf. on Humanoid Robots*, pp. 394–400, 2014.

[10] E. R. Westervelt, J. W. Grizzle, C. Chevallereau, J. H. Choi, and B. Morris, *Feedback Control of Dynamic Bipedal Robot Locomotion*, CRC Press, 2007.